

# Cocrystals of Atomically Precise Noble Metal Nanoclusters

Mohammad Bodiuzzaman, Wakeel Ahmed Dar, and Thalappil Pradeep\*

Cocrystallization is a phenomenon involving the assembly of two or more different chemical entities in a lattice, occurring typically through supramolecular interactions. In this concept, recent advancements in the cocrystallization of atomically precise noble metal clusters and their potential future directions are presented. Different strategies to create coassemblies of thiolate-protected noble metal nanoclusters are presented first. An approach is the simultaneous synthesis, and cocrystallization of two clusters having similar structures. A unique pair of clusters found recently, namely Ag<sub>40</sub> and Ag<sub>46</sub> with same core but different shell are taken to illustrate this. In another category, the case of the same core is presented, namely Ag<sub>116</sub> with different shells, as in a mixture of Ag<sub>210</sub> and Ag<sub>211</sub>. Next, an intercluster reaction is presented to create cocrystals through selective crystallization of the reaction products. The coexistence of competing effects, magic sizes, and magic electron shells in a coassembly of alloy nanoclusters is discussed next. Finally, an assembly strategy for nanoclusters using electrostatic interactions is described. This concept is concluded with a future perspective on the emerging possibilities of such solids. Advancements in this field will certainly help the development of novel materials with exciting properties.

bridging link between atoms and bulk state of materials. NCs have precise molecular formulae and possess many properties that are similar to those of molecules (e.g., quantized energy levels, optical absorption, and emission, nonlinear optical properties, electrochemical properties, chirality, and magnetism).<sup>[4,8,9]</sup> The properties of NCs depend heavily on their size, geometry, and composition, due to the quantum confinement effects.<sup>[10]</sup> They also vary drastically with the number of constituting atoms. This has greatly strengthened the importance of cluster chemistry.<sup>[11]</sup>

Among the NCs, the most important family of stable clusters belong to those of noble metals, typically protected with thiolates. Considering the affinity of thiols toward gold or silver, Brust et al.<sup>[12,13]</sup> have introduced thiols as ligands, and the era of monolayer protected clusters was born with thiol protection. Till date many clusters have been synthesized following the

modified Brust synthesis method.

Single crystal X-ray structures are considered as the holy grail of cluster science. More than 500 clusters (as on June 2020) have single crystal structures.<sup>[3,5,15,16]</sup> Exploring the total structures of metal NCs is of great significance for explaining their stability, metal sulfur interface, and different properties. Nanoclusters are generally represented as M<sub>x</sub>(SR)<sub>y</sub> (where *x* and *y* represent the number of metal atoms and protecting ligands, respectively, and the latter are typically thiols, and they bind to the metal surface as thiolate, -SR). Nanoclusters can also be stabilized by thiol-phosphine mixtures. Thiol is used to provide primary protection to the cluster, and phosphine acts as a secondary ligand. In presence of multiple ligands, stability and properties of NCs were enhanced than those composed of single ligands.<sup>[6]</sup> Particularly, secondary ligands help in crystallizing molecules as well as enhancing their optical properties.<sup>[17,18]</sup> After synthesis, the most important effort is to understand the cluster with molecular tools, such as mass spectrometry to assign the precise composition. Subsequently, the purified and often size separated cluster is assembled leading to a well-ordered crystal. A number of techniques can be used to understand the composition and structure. This approach is depicted in **Scheme 1**. Atomic-level doping of foreign metals in the parent cluster is known to create doped or alloy clusters, which exhibit enhanced stability and improved optical and catalytic properties.<sup>[19]</sup> Precise molecular structure, electronic energy levels, optical absorption and emission,<sup>[10]</sup> reactivity,<sup>[20,21]</sup> electroreduction,<sup>[22]</sup> water oxidation,<sup>[23]</sup> sensing,<sup>[24,25]</sup> bioimaging,<sup>[26]</sup> catalysis,<sup>[22,27]</sup> and an expanding

## 1. Introduction

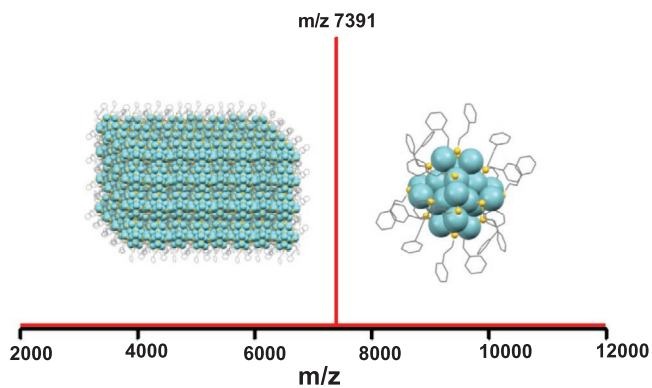
### 1.1. Monolayer Protected Clusters

Atomically precise nanoclusters (NCs) may be defined as nanomaterials composed of a specific number of constituent atoms, typically metals, held together by metal–metal bonds as in Au<sub>25</sub>, Au<sub>38</sub>, Au<sub>102</sub>, Au<sub>144</sub>, Ag<sub>25</sub>, Ag<sub>29</sub>, Ag<sub>44</sub>, and PdAu<sub>24</sub> with fixed number of ligands and precise charges, so that the overall entity has a well-defined composition, structure, and associated properties.<sup>[1–7]</sup> Nuclearity of the cluster is the number of metal atoms in this core which has a diameter in the range of 1–3 nm. NCs behave like molecules and are not generally plasmonic in nature and exhibit optical properties distinctly different from those of traditional nanoparticles. Bonding between the atoms in NCs is different from those in bulk metals or in nanoparticles. Their sizes (<3 nm) fall between atoms and nanoparticles, and therefore, this regime of matter is considered as the

Dr. M. Bodiuzzaman, Dr. W. A. Dar, Prof. T. Pradeep  
Department of Chemistry  
DST Unit of Nanoscience and Thematic Unit of Excellence  
Indian Institute of Technology Madras  
Chennai 600036, India  
E-mail: pradeep@iitm.ac.in

 The ORCID identification number(s) for the author(s) of this article can be found under <https://doi.org/10.1002/smll.202003981>.

DOI: 10.1002/smll.202003981



**Scheme 1.** An atomically precise cluster characterized by molecular tools, such as mass spectrometry, is assembled to give a cluster crystal. For illustration, the cluster used here is  $\text{Au}_{25}(\text{SCH}_2\text{CH}_2\text{C}_6\text{H}_5)_{18}^-$ . The ligand employed here,  $\text{C}_6\text{H}_5\text{CH}_2\text{CH}_2\text{SH}$  or phenylethanethiol, binds to the cluster core as phenylethanethiolate,  $\text{C}_6\text{H}_5\text{CH}_2\text{CH}_2\text{S}^-$ , referred to as PET). Mass spectrum. Reproduced with permission.<sup>[14]</sup> Copyright 2017, American Chemical Society.

body of emerging properties, increasingly reaffirm the molecular nature of such systems. For specific aspects of cluster synthesis, characterization, and crystallization, please consult other articles in this special issue on clusters.

## 1.2. Cluster Crystals

Assembling such clusters with similar molecular entities has been explored from the very early period of cluster science, and the very first example of gold clusters protected with phosphine was cocrystallized with a Keggin anion,  $\alpha\text{-}[\text{PW}_{12}\text{O}_{40}]^{3-}$  in 2006.<sup>[28]</sup> Coassemblies composed of fullerenes and clusters of cobalt and iron have been reported subsequently.<sup>[29,30]</sup> Recently, Roy group reported superconductivity in cluster assembled solids of  $\text{Re}_6\text{Se}_8\text{Cl}_2$ .<sup>[31]</sup> The emergence of thiolated gold clusters with chemical and physical stability, exhibiting new properties, such as distinct optical absorption and visible to near-infrared emission present new possibilities for their assembled solids. Existence of well-defined cluster shapes derived from polyhedra belonging to different categories and the presence of covalently anchored ligands on metal cores, capable of making specific noncovalent interactions between protected clusters and possibilities of inclusion complexes with ligands, together expand the possibility of assembly of thiolated noble metal clusters.<sup>[32,33]</sup>

Cocrystallization is a well-known approach used for the design of diverse new multicomponent solids. Current attraction of cocrystals is mainly due to their applications in pharmaceuticals in terms of modifying the physicochemical properties of drugs.<sup>[35]</sup> A few examples of cocrystals of small molecules are presented in **Table 1**. They have multiple advantages as follows: a) Novelty: Cocrystallization leads to unique solids in terms of their structures and properties. b) Utility: Cocrystals show different physicochemical properties which have been exploited for specific and wide-ranging applications as in electronics, solar cells, energy storage, and luminescent materials. c) Multiplicity: A large number of products are possible as thousands of organic compounds can make cocrystals. d) Greenness: The accessibility of hundreds of

precursors for cocrystallization and comparatively easy synthetic methods lead to the saving of energy, effort, and time.

In the recent past, we find that research on cocrystallization is expanding from pharmaceuticals to materials. Cocrystallization of different NCs could lead to potential new physicochemical properties differing from those of their simple physical mixtures. In such a physical mixture, the periodicity of building blocks and associated ordered supramolecular interactions will be absent which can bring modification in mechanical properties, optical and electrical transport properties as physical properties, such as melting point. Cocrystals of clusters reported are listed in **Table 1**. The concept of cocrystallization is very new in thiolate-protected atomically precise nanoclusters. Emerging examples for such systems are beginning to be available, and a rich diversity in this category of materials is definite to make a lasting impact in chemical science. In this Concept, we explore the new directions of this emerging science, manifested in noble metal cluster cocrystals. These are as follows:

- i) Simultaneous encapsulation of externally similar structures in a single crystal.
- ii) Selective crystallization from a reaction mixture as a result of interparticle reaction.
- iii) Coexistence of competing effects (magic sizes vs magic electron shells) in alloy nanoparticles to form cocrystals.
- iv) Cocrystals composed of +ve and -ve clusters making an ionic cluster solid.

These aspects are summarized in **Scheme 2**. In the sections below, we discuss each of these specific categories.

## 2. Simultaneous Encapsulation of Similar Structures in a Single Crystal

A large number of atomically precise metal nanoclusters are crystallized in the recent past.<sup>[3,6,56-64]</sup> They can be understood by the divide and protect rule<sup>[65]</sup> in which metallic cores are surrounded by a polymeric shell, usually made by staple motifs. In general, clusters are formed starting with well-known icosahedral cores with appropriate capping and protecting linkages, often arranged as monomeric (-SR-M-SR-) or dimeric (-SR-M-SR-M-SR-), etc., staples. The staple linkage around the core is called a shell. Among gold clusters,  $\text{Au}_{25}(\text{SR})_{18}$  is an intensely studied one because of its versatility toward ligands. It consists of an  $\text{Au}_{13}$  icosahedral core, protected by 6  $\text{Au}_2(\text{SR})_3$  staples making a  $\text{Au}_{12}\text{SR}_{18}$  shell (**Figure 1A**).<sup>[4]</sup> Similar core and shell structure was observed in  $\text{Ag}_{25}(\text{SR})_{18}$  by the Bakr group.<sup>[62]</sup>  $\text{Ag}_{29}(\text{S}_2\text{R})_{12}(\text{PPh}_3)_4$ , another intensely studied cluster system consists of the  $\text{Ag}_{13}$  icosahedral core and  $\text{Ag}_{16}\text{S}_{24}\text{P}_4$  shell. These core and shell structures are summarized in **Figure 1**. Other core structures, namely, face-centered cube, simple cube, biicosahedra, body centered cube, and multiple metallic layer core structures have also been observed.<sup>[58,61,66-69]</sup> Combined unit of the core and shell structures create 3D atomic structures of clusters. This molecular framework with structural rigidity is also associated with magic electronic structure, to ensure that such systems are stable.<sup>[70]</sup> Understanding of such structures

**Table 1.** Some examples of cocrystals of small molecules, clusters, and their importance. In the category of small molecules, only illustrative examples are given.

Type	Cocrystals	Importance	Ref.
Small molecules	Cis-itraconazole and 1,4-dicarboxylic acids, Vitamins D <sub>2</sub> (VD <sub>2</sub> ) and D <sub>3</sub> (VD <sub>3</sub> ), hexamethylenebisacetamide and aliphatic even-numbered dicarboxylic acids, aspirin and 4,4'-bipyridine, fluoxetine hydrochloride and benzoic acid, fluoxetine hydrochloride and fumaric acid, acetaminophen with theophylline, acetaminophen and its hydrochloride salt	Pharmaceutical applications	[34–40]
	1,2-bis(2-methyl-5-(1-naphthyl)-3 thienyl)perfluorocyclopentene and perfluoronaphthalene	Converts light into mechanical work	[41]
	2,4,6,8,10,12-hexanitro-2,4,6,8,10,12-hexaazaiso-wurtzitane and 2,4,6-trinitrotoluene (TNT)	Smart materials	[42]
	Anthracene and tetracene	Novel fluorophores for solar concentrators	[43]
	Gallic acid and isoniazid	Structural insights into proton conduction	[44]
	2,7-di-tert-butyl-10,14-di(thiophen-2yl)phenanthro[4,5-abc][1,2,5]thiadiazolo[3,4-i]phenazine and tetracyanoquinodimethane (TCNQ)	Switching of p-type semiconductor to n-type semiconductor	[45]
Caffeine, 4-chloro-3-nitrobenzoic acid and methanol, p-phenylenediamine and N-phenyl-p phenylenediamine	New organic functional materials	[46,47]	
Cocrystals of clusters	[Au <sub>9</sub> (PPh <sub>3</sub> ) <sub>8</sub> ] <sub>2</sub> [V <sub>10</sub> O <sub>28</sub> H] <sub>2</sub>	Crystal structure	[48]
	[(In <sub>3</sub> GeS <sub>7</sub> )(Cu <sub>5</sub> In <sub>30</sub> S <sub>56</sub> )] <sup>18-</sup> [(H <sub>2</sub> TMDP) <sup>2+</sup> ] <sub>9</sub> (TMDP = 4,4'-trimethylenedipiperidine)	Crystal structure	[49]
	[Co <sub>6</sub> Te <sub>8</sub> (PEt <sub>3</sub> ) <sub>6</sub> ][Fe <sub>8</sub> O <sub>4</sub> pz <sub>12</sub> Cl <sub>4</sub> ] (pz = pyrazolate)	Crystal structure	[50]
	[Co <sub>6</sub> Te <sub>8</sub> (PnPr <sub>3</sub> ) <sub>6</sub> ][C <sub>60</sub> ] <sub>3</sub> and [Co <sub>6</sub> Se <sub>8</sub> (PEt <sub>3</sub> ) <sub>6</sub> ][C <sub>60</sub> ] <sub>3</sub>	Electronic transport properties	[30]
Recent trends in cocrystallization of thiolate-protected noble metal nanoclusters	(Ag <sub>210</sub> (iPr <sub>3</sub> PhS) <sub>71</sub> (Ph <sub>3</sub> P) <sub>5</sub> Cl and Ag <sub>211</sub> (iPr <sub>3</sub> PhS) <sub>71</sub> (Ph <sub>3</sub> P) <sub>6</sub> Cl	Crystal structure	[51]
	[Ag <sub>46</sub> (SPhMe <sub>2</sub> ) <sub>24</sub> (PPh <sub>3</sub> ) <sub>8</sub> ] <sup>2+</sup> and [Ag <sub>40</sub> (SPhMe <sub>2</sub> ) <sub>24</sub> (PPh <sub>3</sub> ) <sub>8</sub> ] <sup>2+</sup>	Crystal structure	[52]
	[(AuAg) <sub>267</sub> (SR) <sub>80</sub> ] and [(AuAg) <sub>45</sub> (SR) <sub>27</sub> (PPh <sub>3</sub> ) <sub>6</sub> ]	Crystal structure	[53]
	[Ag <sub>16</sub> (S <sup>t</sup> Bu) <sub>8</sub> (CF <sub>3</sub> COO) <sub>7</sub> (ACN) <sub>3</sub> Cl] <sup>+</sup> [Ag <sub>17</sub> (S <sup>t</sup> Bu) <sub>8</sub> (CF <sub>3</sub> COO) <sub>7</sub> (ACN) <sub>3</sub> Cl] <sup>+</sup>	Reaction and cocrystallization	[54]
	[Ag <sub>26</sub> Au(2-EBT) <sub>18</sub> (PPh <sub>3</sub> ) <sub>6</sub> ] <sup>+</sup> and [Ag <sub>24</sub> Au(2-EBT) <sub>18</sub> ] <sup>-</sup>	Ionic cocrystal	[55]

obviously shows the appearance of common outer shell having varied inner cores and vice versa.

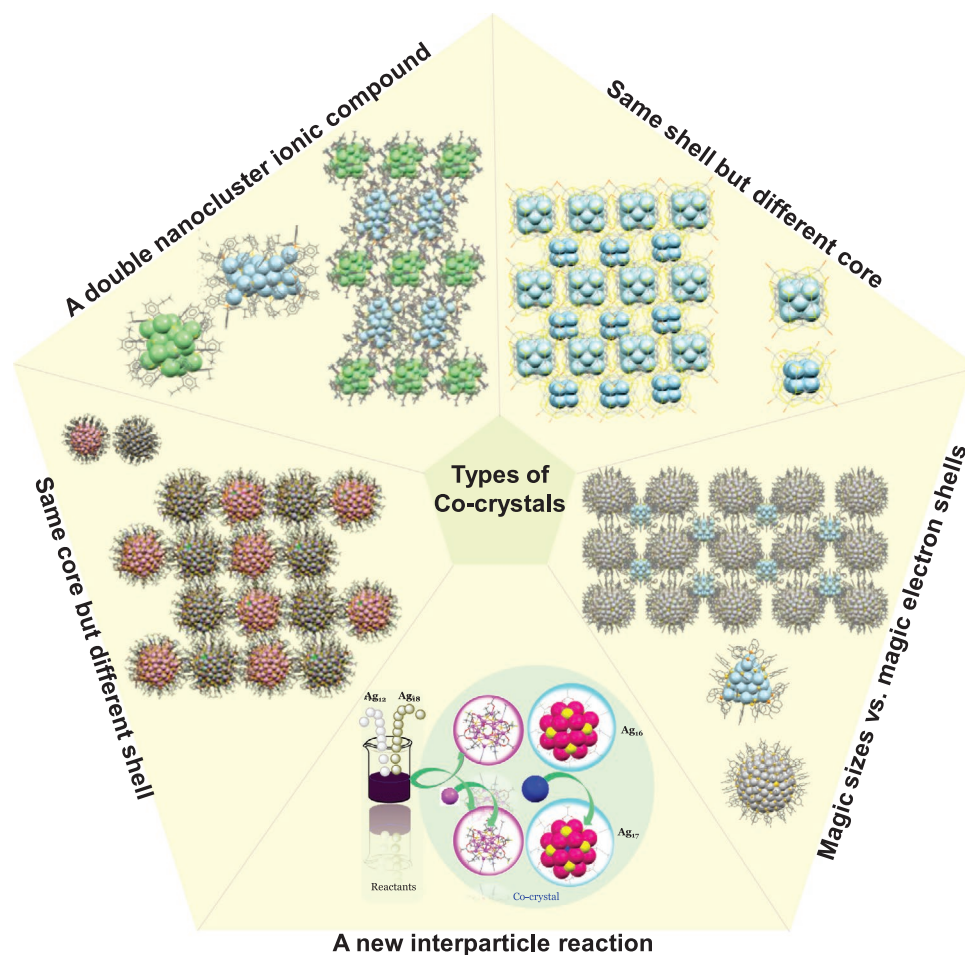
### 2.1. Same Shell but Different Core

Mixed ligand protected molecular pieces of silver, namely, [Ag<sub>46</sub>(DMBT)<sub>24</sub>(TPP)<sub>8</sub>](NO<sub>3</sub>)<sub>2</sub> and [Ag<sub>40</sub>(DMBT)<sub>24</sub>(TPP)<sub>8</sub>](NO<sub>3</sub>)<sub>2</sub> (shortened as Ag<sub>46</sub> and Ag<sub>40</sub>, respectively) with the same shell but different inner cores were synthesized simultaneously.<sup>[52]</sup> A mixture of purified clusters was crystallized in a monoclinic crystal system with space group, C2/m.

Structural refinement unambiguously confirmed that there are two types of clusters in the crystal. These clusters exhibited almost the same structures but differed by six metals in them and can exchange their positions. Total structures of both the clusters revealed that six atomic locations of the core of [Ag<sub>46</sub>(DMBT)<sub>24</sub>(TPP)<sub>8</sub>] are empty in [Ag<sub>40</sub>(DMBT)<sub>24</sub>(TPP)<sub>8</sub>]. Due to identical structures of the outer shell, clusters were not able to differentiate themselves and got cocrystallized. Therefore, the difference in the inner core does not affect the

growth process of the crystals, and both the clusters got nucleated in equal proportions in a single crystal. An examination of the clusters [Ag<sub>40</sub>(DMBT)<sub>24</sub>(TPP)<sub>8</sub>] and [Ag<sub>46</sub>(DMBT)<sub>24</sub>(TPP)<sub>8</sub>] revealed simple cubic (Ag<sub>8</sub>) and face-centered cubic (Ag<sub>14</sub>) structures, respectively, as the inner cores. These inner cores are protected by a common outer shell, [Ag<sub>32</sub>(DMBT)<sub>24</sub>(TPP)<sub>8</sub>] to form the molecular architecture. The structures of the inner core and outer shell are presented in **Figure 2A–D**. Both the clusters were assembled in exactly the same fashion to form the solid (**Figure 2G,H**). In a unit cell, there are two molecules which are connected through supramolecular interactions. In two dimensional lattices, both the clusters were assembled in the same way. Ag<sub>40</sub> was packed into centered rectangular and rectangular 2D lattices along the z and x directions, respectively. The same packing was seen for Ag<sub>46</sub> also.

Encapsulation of those clusters in a single crystal was further proved by high resolution mass spectrometry (HR ESI MS). ESI MS of a crystal dissolved in methanol showed multiple peaks which were assigned as Ag<sub>40</sub><sup>2+</sup>, Ag<sub>40</sub><sup>3+</sup>, and Ag<sub>46</sub><sup>2+</sup> (with the ligand structure intact). Collision induced dissociation studies were performed to confirm the compositions.



**Scheme 2.** Schematic representation of the concepts of emerging science manifested in noble metal cluster cocystals. The image of interparticle reaction is reproduced with permission.<sup>[91]</sup> Copyright 2019, American Chemical Society.

## 2.2. Same Core, Different Shell

Another category of encapsulation of similar structures is one with the same metallic core with a different shell. In this concept, a ligand control methodology was developed to synthesize two silver nanoparticles, namely  $\text{Ag}_{210}$  and  $\text{Ag}_{211}$ , which were crystallized in one crystal. They contain the same pseudofivefold symmetric  $\text{Ag}_{116}$  core, which is made of three shells like  $\text{Ag}_{19}@\text{Ag}_{52}@\text{Ag}_{45}$  (Figure 3A–C).  $\text{Ag}_{19}$  consists of three shared pentagonal bipyramidal structures (Figure 3A).  $\text{Ag}_{52}$  is made of six layers of silver atoms, top and bottom layers contain pentagonal pyramids, and in-between, it has four  $\text{Ag}_{10}$  layers (Figure 3C). Three chain-like layers of  $\text{Ag}_{15}$  construct  $\text{Ag}_{45}$  (Figure 3C).  $\text{Ag}_{116}$  core is covered by shells of  $\text{Ag}_{89}(\text{SR})_{71}\text{Cl}[\text{Ag}(\text{Ph}_3\text{P})]_5$  and  $\text{Ag}_{89}(\text{SR})_{71}\text{Cl}[\text{Ag}(\text{Ph}_3\text{P})]_6$  to create  $\text{Ag}_{210}$  and  $\text{Ag}_{211}$ , respectively (Figure 3). These shells are formed by combining different irregular geometrical structures which make them distorted.

Single crystal X-ray diffraction (SCXRD) analysis clearly showed that both the particles have exactly the same core of  $\text{Ag}_{116}$  but differ in shell structure by a unit of silver phosphine complex. This slight change in the secondary ligands resulted in the formation of two distinct particles. In  $\text{Ag}_{211}$ , five  $[\text{Ag}(\text{Ph}_3\text{P})]$  units are bonded to the core at corners of the

pentagon, also called as equatorial positions, perpendicular to the fivefold axis (Figure 3F). The sixth  $\text{AgPPh}_3$  is bonded at the middle of the pentagon and parallel to the fivefold axis, called a polar site (Figure 3F). The pentagon is shown with a green dotted line in Figure 3F. In  $\text{Ag}_{210}$ , one corner of the pentagon is missing; other sites of shell are the same as that of  $\text{Ag}_{211}$  (Figure 3G). However, this one unit change of  $\text{AgPPh}_3$  complex in the shell structure did not affect the growth process during crystallization of  $\text{Ag}_{210}$  and  $\text{Ag}_{211}$ . Seemingly, a large core in both particles enables the cocrystal formation. Another example of this type is made of  $\text{Pt}_1\text{Ag}_{28}(\text{S-Adm})_{20}$  and  $\text{Pt}_1\text{Ag}_{28}(\text{S-Adm})_{18}(\text{HOS-Adm})_2$  (S-Adm is denoted as adamantanethiolate). Hydroxyl group on the surface creates such type of structural diversity.<sup>[71]</sup>

## 3. Selective Crystallization from a Reaction Mixture Leading to Cocystals by a New Type of Interparticle Reaction

Chemical reaction of clusters or interparticle reactions is a new class of reactions first observed by our group, which explains the interchange of metals and protecting ligands between

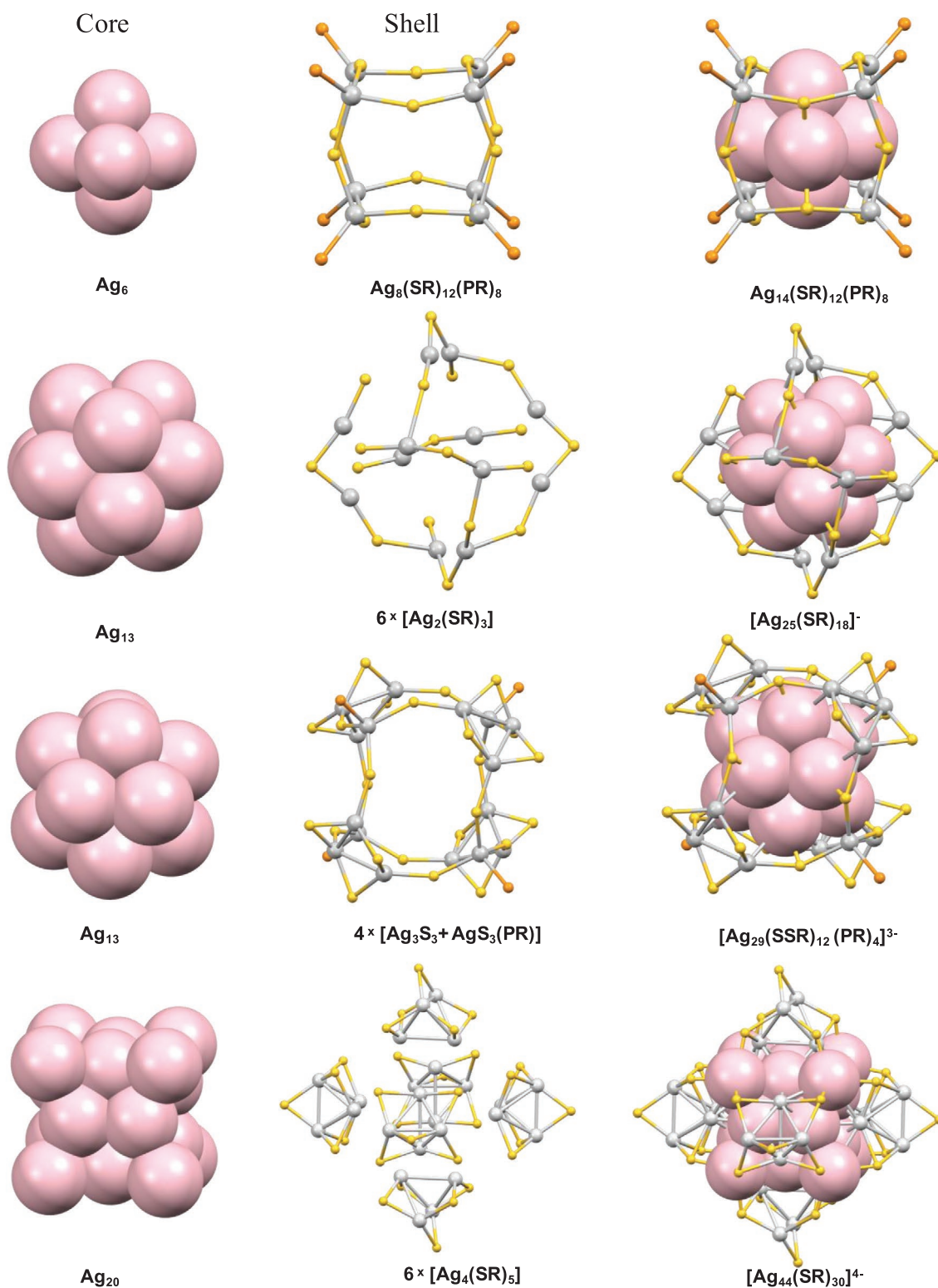


**Figure 1.** Crystal structures of three well-known clusters to understand core and shell structure. Colors and diameters of core and staple atoms of shown differently to understand the structural motifs clearly.

different atomically precise clusters, resulting in the formation of new clusters.<sup>[20,72]</sup> Such types of reactions were carried out by reacting ligand protected clusters made of different metal

atoms, for example, Ag and Au NCs. Reaction between Au<sub>25</sub> and Ag<sub>44</sub> was the first to be reported, followed by the reaction of Ag<sub>25</sub> and Au<sub>25</sub>.<sup>[72]</sup> In such reactions, a series of alloy clusters

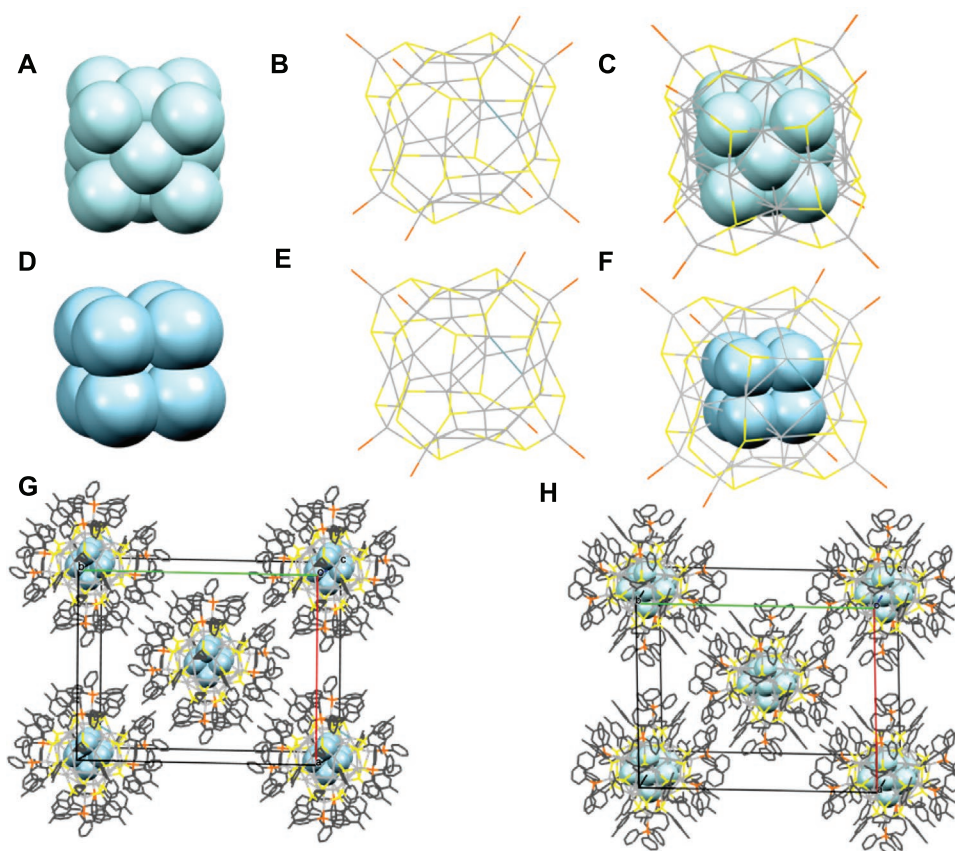


**Figure 2.** Structural anatomy of  $[Ag_{40}(SPhMe_2)_{24}(PPh_3)_8]$  and  $[Ag_{46}(SPhMe_2)_{24}(PPh_3)_8]$  clusters. A,D)  $Ag_8$  and  $Ag_{14}$  inner core structures (the metal structure that is not connected to ligands) of  $[Ag_{40}(SPhMe_2)_{24}(PPh_3)_8]$  and  $[Ag_{46}(SPhMe_2)_{24}(PPh_3)_8]$ , respectively.  $Ag_8$  and  $Ag_{14}$  correspond to simple cubic and face-centered cubic structures, respectively. B,E) Common shell,  $Ag_{32}S_{24}P_8$ , structures of the clusters without inner cores. C,F) The structures of  $[Ag_{40}S_{24}P_8]$  and  $[Ag_{46}S_{24}P_8]$ , respectively. G,H) Organization of  $Ag_{40}$  and  $Ag_{46}$ , respectively, in a unit cell.

were formed. In this context, it is important to mention another methodology to create alloy NCs is antigalvanic reaction. In this process, more noble metal ions are reduced by less noble metal.<sup>[73]</sup> In intercluster reaction, both galvanic and antigalvanic reactions occur simultaneously. Many interparticle reactions using different clusters have been explored.<sup>[74–79]</sup> In view of this, our group was interested in creating new mixed-solids by extending our previous work. A homometallic interparticle reaction methodology was developed to synthesize new NCs.

Interparticle reaction was studied between nanoclusters containing similar metal atoms such as  $[Ag_{12}(S^tBu)_8(CF_3COO)_5(ACN)]^+$  denoted as  $Ag_{12}$ , ( $S^tBu$  = tert-butylthiolate,  $CF_3COO$  = trifluoroacetate) and  $[Ag_{18}(TPP)_{10}H_{16}]^{2+}$  denoted as  $Ag_{18}$ , (TPP = triphenylphosphine) resulting in the formation of two product nanoclusters viz.,  $[Ag_{16}(S^tBu)_8(CF_3COO)_7(ACN)_3Cl]^+$  and  $[Ag_{17}(S^tBu)_8(CF_3COO)_7(ACN)_3Cl]^+$  denoted as  $Ag_{16}$  and  $Ag_{17}$ , respectively. Interestingly, in a single crystal, the populations of  $Ag_{16}$  and  $Ag_{17}$  were in the ratio of 2:1 and in the product mixture, however, equal population (1:1) was observed. These results have been confirmed by SCXRD and HR ESI MS. Therefore, this type of reaction suggests the formation of a cocrystal, involving selective crystallization. Seemingly, selective crystallization happened because of the enhanced stability

of solids at a particular ratio. The ratio of nanoclusters in the solid is determined by their potential energy minimum. We tried to prove the existence of equal concentrations of  $Ag_{16}$  and  $Ag_{17}$  NCs in the solution by nuclear magnetic resonance spectroscopy but due to their same shell structures, useful information could not be obtained. We attempted to separate the component clusters by high performance liquid chromatography (HPLC) and thin layer chromatography (TLC) but it was also unsuccessful. In HPLC and TLC procedures, clusters were degraded on the column and TLC plate, respectively. This inability did not surprise us as while HPLC and TLC are well known for gold clusters, very few reports exist for silver clusters.

ESI MS of the product solution in positive ion mode shows the formation of NCs in the solution with  $m/z$  at 3055, 3277, and 3499, corresponding to  $[Ag_{17}(S^tBu)_8(CF_3COO)_7(ACN)_3Cl]^+$ ,  $[Ag_{16}(S^tBu)_8(CF_3COO)_6(ACN)_3Cl]^+$ , and  $[Ag_{15}(S^tBu)_8(CF_3COO)_5(ACN)_3Cl]^+$ , respectively (Figure 4A). The peak separation is  $m/z$  1.00, for each of the clusters indicating +1 charge state of the NCs. The formation of NCs was verified by matching their isotopic distributions as shown at the inset of Figure 4A. The stability of peaks was further analyzed using collision-induced dissociation (CID) experiments on the peaks with  $m/z$  3277 and 3499. Analysis of CID studies showed

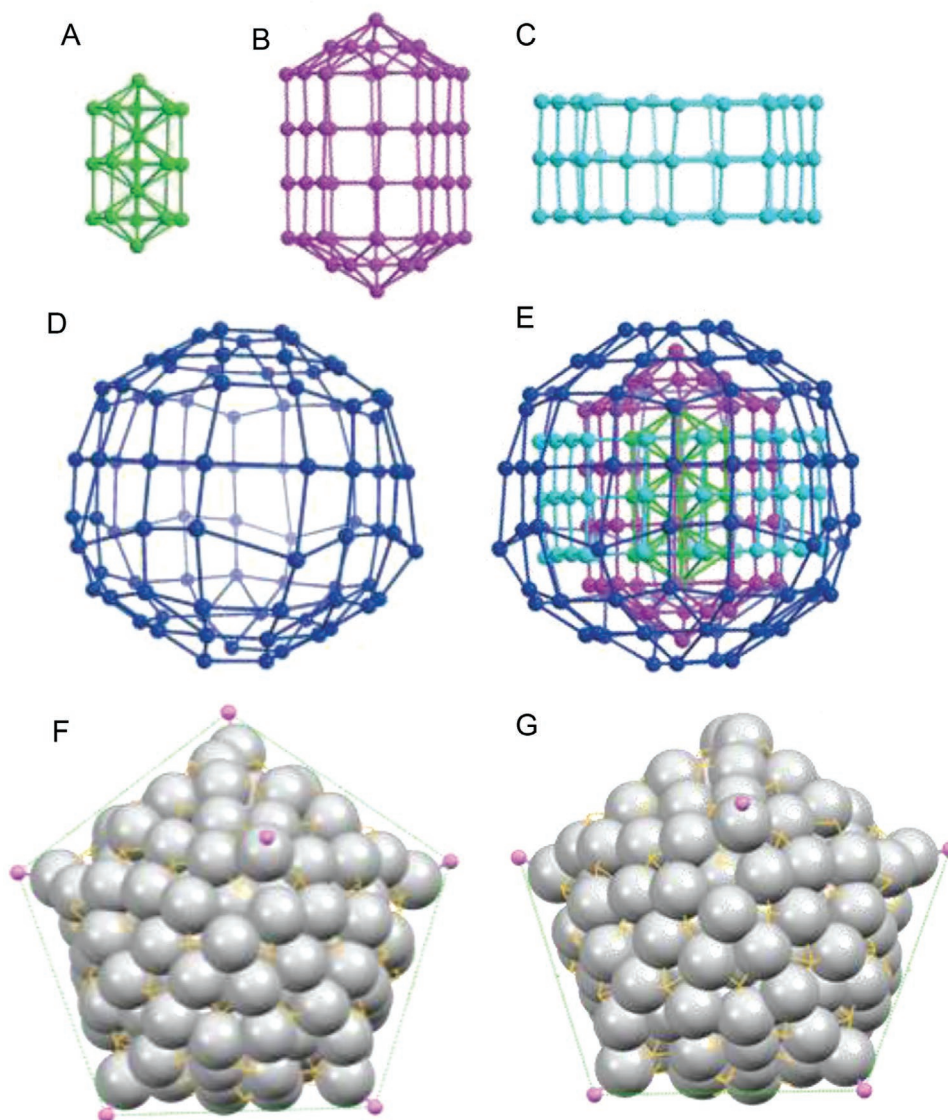


**Figure 3.** Common core structures present in Ag<sub>210</sub> and Ag<sub>211</sub>. A) Ag<sub>19</sub>, B) Ag<sub>52</sub>, C) Ag<sub>45</sub> pentagonal cylinder, D) Outermost Ag<sub>89</sub> shell, and E) Full shell structure Ag<sub>19</sub>@Ag<sub>52</sub>@Ag<sub>45</sub>@Ag<sub>89</sub>. F,G) Structures of Ag<sub>211</sub> and Ag<sub>210</sub>, respectively. Reproduced with permission.<sup>[51]</sup> Copyright 2019, Wiley-VCH.

that Ag<sub>15</sub> was the fragmented peak of Ag<sub>16</sub> due to the loss of CF<sub>3</sub>COOAg. However, CID measurements of *m/z* 3499 (Ag<sub>17</sub>) showed the removal of ligands alone with increasing collision energy, indicating that Ag<sub>16</sub> was a discrete entity. Therefore, CID studies showed that the solution had two types of NCs (Ag<sub>16</sub> and Ag<sub>17</sub>). The populations of peaks corresponding to Ag<sub>16</sub> and Ag<sub>17</sub> in product solution and crystals dissolved in acetonitrile are in 1:1 and 2:1, respectively. ESI MS of the supernatant after crystallization showed peaks at the same *m/z*, similar to those obtained from crystal and product solutions, although with unequal populations. These results suggested that a single crystal showed selective crystallization of 2:1 of Ag<sub>16</sub> and Ag<sub>17</sub> NCs, respectively, even though the NCs were of equal concentrations in the product solution. An attempt to isolate these NCs was made using different synthetic protocols, but we were unable to succeed in this case. This reaction is the first

reaction where interparticle reaction between silver NCs resulted in product cocrystals by selective crystallization. A balanced chemical equation was written based on the findings from ESI MS and SCXRD data (considering the contribution of silver and sulfur atoms alone) (Scheme 3).

ESI MS intensities of the product solution and the supernatant obtained after crystallization provide evidence for a balanced chemical reaction. From ESI MS, equal populations of NCs in the product solution got changed into 2:1 in the crystal (Ag<sub>16</sub>:Ag<sub>17</sub>). ESI MS of the supernatant, after crystal formation, showed increased intensity of Ag<sub>17</sub>, even though the ratio was not 1:2, which was attributed to the preferential incorporation of the clusters in the crystals. The formation of cocrystal nanoclusters arising from interparticle reactions was studied using time-dependent ESI MS and UV-vis spectroscopy. Studies were carried out at different time intervals, *t* = 2, 5, 15, 30, and

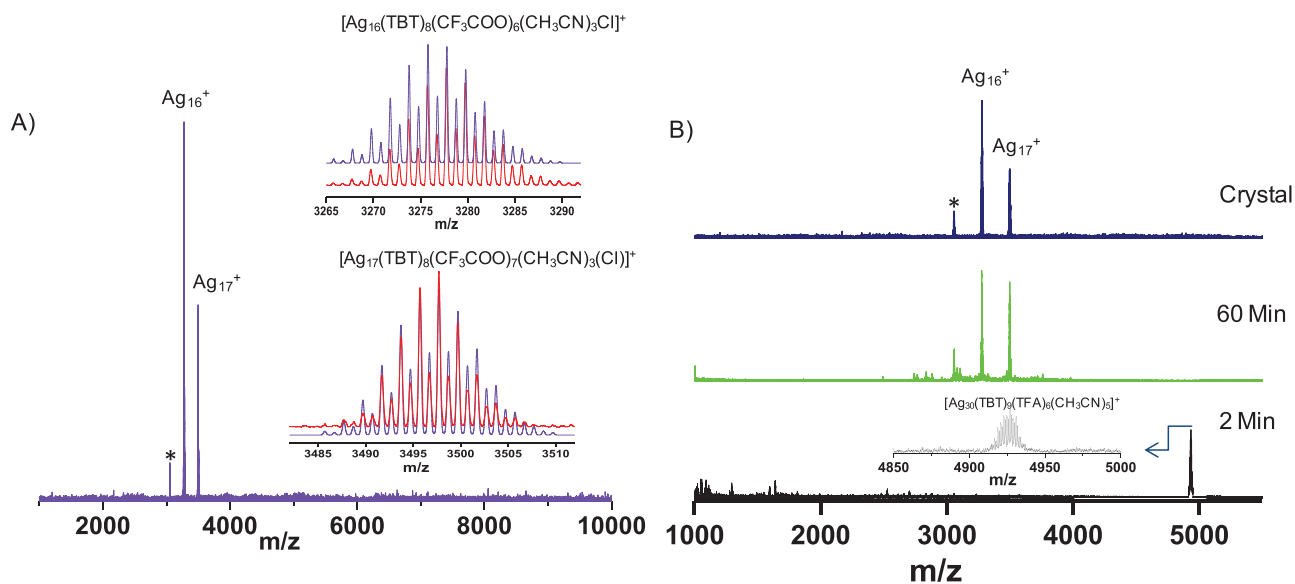


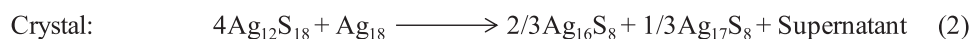
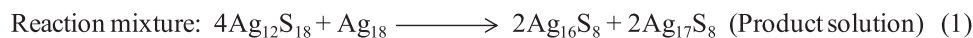
**Figure 4.** A) ESI MS of crystals of a mixture of  $\text{Ag}_{16}$  and  $\text{Ag}_{17}$  dissolved in acetonitrile. Major peaks are assigned as  $[\text{Ag}_{17}(\text{S}^i\text{Bu})_8(\text{CF}_3\text{COO})_7(\text{ACN})_3(\text{Cl})]^+$  and  $[\text{Ag}_{16}(\text{S}^i\text{Bu})_8(\text{CF}_3\text{COO})_6(\text{ACN})_3(\text{Cl})]^+$ . Isotopic distributions of the experimental spectra (violet trace) are compared with the simulated spectra (red trace) in the inset. B) ESI MS spectra as a function of time of the reaction mixture during the synthesis of  $\text{Ag}_{16}^+$  and  $\text{Ag}_{17}^+$ . Peak marked as \* corresponds to the loss of  $\text{CF}_3\text{COOAg}$ . Reproduced with permission.<sup>[54]</sup> Copyright 2019, American Chemical Society.

60 min, and 7 days after the reaction. ESI MS measurements in the positive ion mode showed that individual peaks corresponding to  $\text{Ag}_{12}$  and  $\text{Ag}_{18}$  did not appear. ESI MS recorded after 2 min of the reaction showed that a distinctive peak at  $m/z$  4928 emerged whose molecular mass was equal to that of  $[\text{Ag}_{30}(\text{S}^i\text{Bu})_9(\text{CF}_3\text{COO})_6(\text{ACN})_5]^+$ , abbreviated as  $\text{Ag}_{30}$ , indicating that an addition reaction had taken place between the reactant nanoclusters (Figure 4B). During the reaction, low molecular weight species having  $m/z < 1000$  appeared, which could be due to the formation of thiolates and phosphines. After 5 min of the reaction, ESI MS showed the appearance of many new peaks in the region between  $m/z$  1000–3000, corresponding to short lived intermediate species formed during the reaction, and the peak at  $m/z$  4928 disappeared suggesting its conversion to lower molecular mass intermediates. This may be interpreted as a top-down approach in synthesis. From the time,  $t = 15$ –30 min, ESI MS shows a dynamic change during the reaction and a color change was visible. After 30 min of the reaction, three characteristic peaks emerged whose  $m/z$  values at 3499, 3277, and 3055 corresponded to  $[\text{Ag}_{17}(\text{S}^i\text{Bu})_8(\text{CF}_3\text{COO})_7(\text{ACN})_3\text{Cl}]^+$ ,  $[\text{Ag}_{16}(\text{S}^i\text{Bu})_8(\text{CF}_3\text{COO})_6(\text{ACN})_3\text{Cl}]^+$ , and  $[\text{Ag}_{15}(\text{S}^i\text{Bu})_8(\text{CF}_3\text{COO})_5(\text{ACN})_3\text{Cl}]^+$ , respectively. The reaction appeared to be completed in 1 h, as evident from the disappearance of the reaction intermediate. Intensities of the peaks corresponding to  $\text{Ag}_{16}$

and  $\text{Ag}_{17}$  increased significantly. ESI MS of a few crystals dissolved in acetonitrile were similar ( $m/z$  3055, 3277, and 3499) to the MS obtained after 1 h of the reaction but with varying intensities. It therefore, suggested that the nanoclusters got formed after 1 h. During the course of the reaction, as many as 21 heteroleptic reaction intermediates denoted by a general formula,  $[\text{Ag}_a(\text{STBU})_b(\text{CF}_3\text{COO})_c(\text{ACN})_d\text{Cl}_e]^+$  where  $a = 6$ –15 and 30,  $b = 2$ –9,  $c = 1$ –6,  $d = 0$ –5, and  $e = 0$ –1 were identified, which underwent various rearrangements via a growth mechanism forming the product nanoclusters,  $\text{Ag}_{16}$  and  $\text{Ag}_{17}$ . These intermediates size focus leading to stable product nanoclusters  $[\text{Ag}_{16}(\text{S}^i\text{Bu})_8(\text{CF}_3\text{COO})_6(\text{ACN})_3\text{Cl}]^+$  and  $[\text{Ag}_{17}(\text{S}^i\text{Bu})_8(\text{CF}_3\text{COO})_7(\text{ACN})_3\text{Cl}]^+$ .

#### 4. Cocrystals Due to Magic Sizes and Magic Electron Shells

Ligand protected nanoclusters of noble metals are synthesized by reducing the complexes formed by metal salts with protecting ligands. A reasonable control over their size and atomic structure is obtained via a complex process which is influenced by various parameters during syntheses, such as the ratio of metal to ligand, temperature, the kinetics of reduction,



**Scheme 3.** Chemical equations of the intercluster reaction.

subsequent steps, in particular size focusing, and cleaning. A common view is that the creation of protected clusters can be arrested during their nucleation or etching when a magic size and composition is formed.<sup>[80]</sup> The factors which can control the production of magic cluster are the following

- i) Suitable surface structures which can protect the metallic core;
- ii) Appropriate atomic packing often observed as spherical structures of concentric shells of polyhedra and
- iii) Closed-shell electronic structure stabilizing smaller nanoclusters by a large highest occupied molecular orbital (HOMO)-lowest unoccupied molecular orbital (LUMO) gap.

The synthetic method chosen can offer some strategies for the creation of magic cores and consequent electronic structures. A mixture of  $(\text{AuAg})_{267}$  and  $(\text{AuAg})_{45}$  was synthesized by reducing a complex of metal precursors and ligands by sodium borohydride at 0 °C. Transmission electron microscopic (TEM)

data revealed that the final product contained two monodisperse particles with significant variation in sizes. Larger particle was around 2.5 nm, and the other one was of 1.1 nm. It was difficult to conclude from the TEM data that it formed a cocrystal or a simple mixture of two different particles. Fortunately, authors were able to get single crystals from the reaction mixture, and TEM data were validated by SCXRD. Single crystal X-ray analysis showed that there were two kinds of molecules,  $(\text{AuAg})_{267}(\text{SR})_{80}$  and  $(\text{AuAg})_{45}(\text{SR})_{27}(\text{PPh}_3)_6$  in the lattice, as shown in **Figure 5A**. Smaller cluster was anisotropic in shape but the larger one was spherical. In order to understand the core structure of  $(\text{AuAg})_{267}(\text{SR})_{80}$ , an analysis was performed by removing the protecting ligands. Geometrical anatomy can be presented by four layers,  $k_0(1)@k_1(12)@k_2(42)@k_3(92)@k_4(120)$ .

Here, it is appropriate to mention the previous work of Mackay, who reported in 1962 a sequence in the close packed assembly of spheres.<sup>[81]</sup> He proposed that an assembly of spheres can form concentric layers of icosahedra; packed on the first layer, composed of a 13 sphere icosahedron. In general,  $n$ th

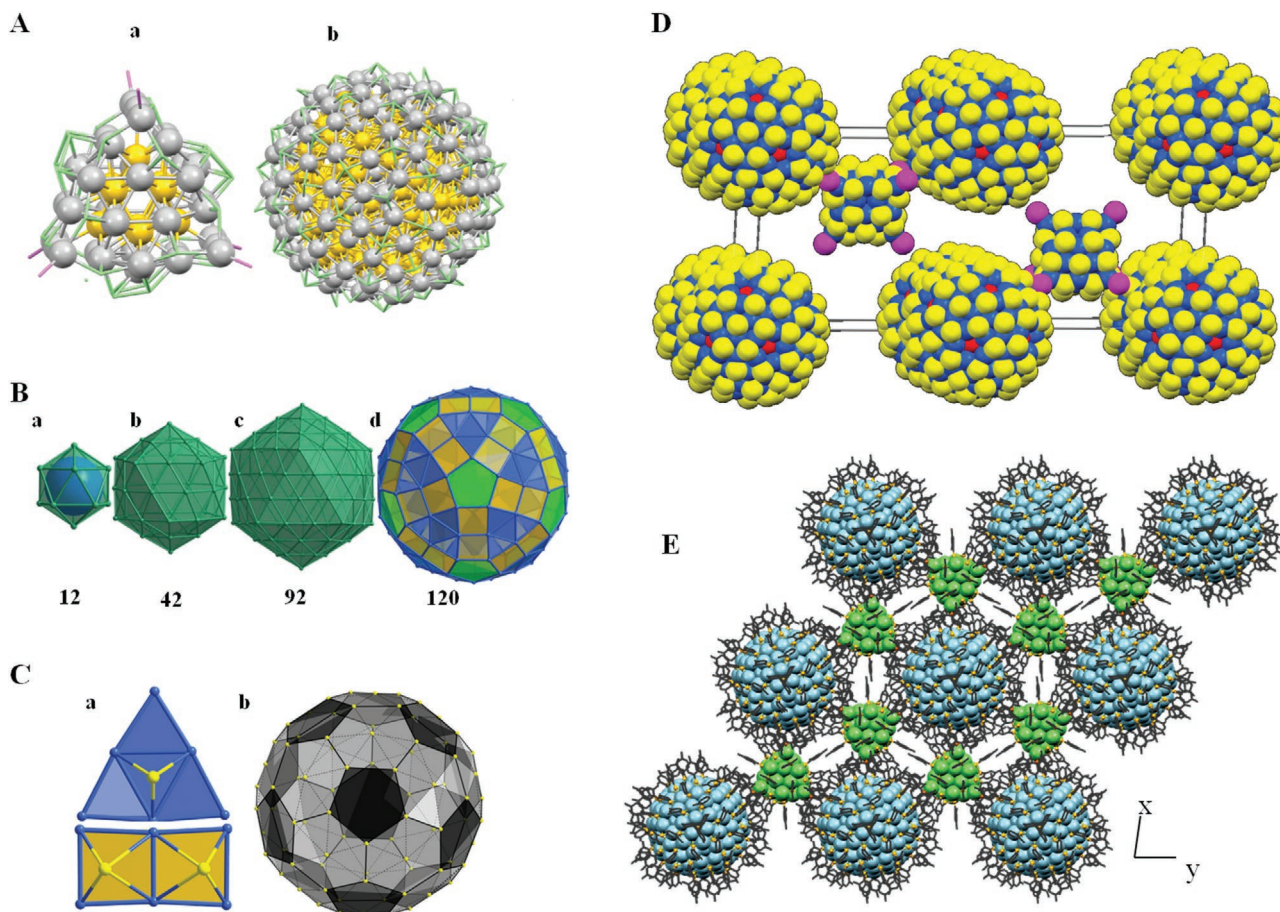


**Figure 5.** A) Crystal structures of component clusters,  $(\text{AuAg})_{45}$  and  $(\text{AuAg})_{267}$ . a) Structures of trigonal prismatic  $(\text{AuAg})_{45}$  and spherical  $(\text{AuAg})_{267}$  nanoparticles. B) Dissection of the metal framework of  $(\text{AuAg})_{267}$  to understand the core structures. Four layers of metal atoms, a–d). a) First Mackay icosahedral core of 12 metal atoms, b) second Mackay layer of 42 metal atoms, c) third Mackay layer of 92 metal atoms, d) fourth anti-Mackay layer of 120 metal atoms. Number of metal atoms is mentioned at the bottom of the structures. Reproduced with permission.<sup>[53]</sup> Copyright 2018, Springer Nature. C) Capping of metal framework by thiolates. a) Triangle and square-like metal structures are capped by sulfur atoms. b) 80 sulfur atoms form buckyball-type structures. Reproduced with permission.<sup>[53]</sup> Copyright 2018, Springer Nature. D) Unit cell representation of  $(\text{AuAg})_{267}$  and  $(\text{AuAg})_{45}$ . There are two units of each particle in the unit cell. Larger components are placed at the corners and edges, while smaller ones are at the inside of the hexagonal unit cell. Reproduced with permission.<sup>[53]</sup> Copyright 2018, Springer Nature. E) Self-assembled packing structure of  $(\text{AuAg})_{45}$  and  $(\text{AuAg})_{267}$ , along z direction.

icosahedral layer is made of  $10n^2 + 2$  spheres (for the 13 sphere icosahedron,  $n = 1$ ). At that time, no crystallographic packing of such types of assemblies was known, and later on  $M_{55}$  clusters were observed in multiple reports which were characterized by mass spectrometry and theoretical studies. It was predicted that  $M_{55}$  contained a  $M_{13}$  (central icosahedron) and a  $M_{42}$  ( $10 \times 2^2 + 2$ ) icosahedral shell, which means it contained two layers of Mackay icosahedra. It was often called as magic cluster system as it had two complete Mackay icosahedra. Over the last decades, the two layer  $M_{55}$  Mackay icosahedron was revealed in various noble metal nanomaterials by SCXRD, namely,  $Pd_{145}$ ,<sup>[82]</sup>  $Pd_{164-x}Pt_x$ ,<sup>[83]</sup>  $Au_{133}$ ,<sup>[60,84]</sup> and  $Pd_{55}$ .<sup>[85]</sup> However, 3rd layer Mackay icosahedron was not observed in these clusters, and it was called an anti-Mackay layer. The major difference between Mackay and anti-Mackay packing structure is in stacking of atoms in the atomic structure. In Mackay, atoms are stacked in face-centered cubic (ABCA...) fashion, and in anti-Mackay, the stacking is hexagonal cubic (ABAB...). It was observed that after successive stacking of Mackay icosahedra (ABCA...), there was stacking faults, i.e., ABA... kind of arrangements.<sup>[86]</sup> This stacking does not follow Mackay's rule, and it is called as anti-Mackay icosahedra. In  $(AuAg)_{267}$ , the next Mackay layer on  $M_{55}$  was observed giving three complete Mackay or magic layers of  $k_0(1)@k_1(12)$  ( $10 \times 1^2 + 2$ )@ $k_2(42)$  ( $10 \times 2^2 + 2$ )@ $k_3(92)$  ( $10 \times 3^2 + 2$ ) to form  $M_{147}$ . The fourth layer,  $k_4(120)$  is not composed of 162 atoms ( $10 \times 4^2 + 2$ ) and therefore not following Mackay's proposed formula and is called as anti-Mackay layer. The three layers are presented as M as it can be Au or Ag. SCXRD refinement revealed that there are positional disorders in their atomic positions. Average occupancies of three layers are not 100% with respect to silver or gold. However, the atoms of fourth layer have 100% average occupancies of Ag. The 120 silver atoms of the fourth layer are bonded to each other to construct a semiregular polyhedron which is made of 20 triangles, 60 squares, and 12 pentagons. The center of every triangle and square face of the fourth layer are connected by thiolates as shown in Figure 5C(a,b). This connectivity occurred in such a way that eighty sulfur atoms form a fullerene-like structure (Figure 5C(b)). The other component of the cocrystal,  $(AuAg)_{45}$  exhibits a shape of trigonal prism, while the larger counterpart is spherical.  $(AuAg)_{45}$  contains  $Au_9$  core inside a trigonal prism of 36 silver atoms to form  $Au_9Ag_{36}$ . There are no Mackay icosahedral cores inside it. Surface silver atoms are protected by  $AgS_3P$  and  $AgS_3$  units. This structure is similar to the previously reported structure of  $Au_9Ag_{36}(SPhCl_2)_{27}(PPh_3)_6$ .<sup>[87]</sup>

It is interesting to see the diversity in terms of the size and shape of the component clusters of the cocrystals. Stabilizing factors are also different as  $(AuAg)_{267}$  is stabilized by magic Mackay icosahedral cores, while geometry of  $(AuAg)_{45}$  does not provide stability. Stability of  $(AuAg)_{45}$  must originate from its electronic structure, which will be discussed later. These diverse  $(AuAg)_{267}$  and  $(AuAg)_{45}$  components serve as the building blocks and were assembled into a 3D structures. The cocrystal forms a hexagonal unit cell and  $(AuAg)_{267}$  molecules form the hexagonal layer (Figure 5D). All the octahedral sites in this structure are filled by  $(AuAg)_{45}$ . SCXRD resolved that in the lattice,  $(AuAg)_{267}$  is neighbored by six  $(AuAg)_{45}$  nanoclusters and vice versa. The main driving force for adopting this kind of packing is strong supramolecular forces between the ligands

of both the particles. Orientations of thiolates of  $(AuAg)_{267}$  and phosphines of  $(AuAg)_{45}$  are perfectly matched to form strong C–H... $\pi$  interactions (at a distance of  $\approx 2.6$  Å).

The electronic structures of both nanoclusters were analyzed by density functional theory which shows the expected HOMO–LUMO gap (0.71 eV) for 18 electrons  $(AuAg)_{45}$  nanocluster. As expected, the closing of the  $1D^{10}$  shell at 18 electrons is indicated by the projection to angular momentum components and after the closing of the  $2S^2$  shell, the energy gap at 20 electrons becomes 0.65 eV. Therefore, the closure of an electron shell at 18 electrons, i.e., at a magic electron number, clearly stabilizes this cluster energetically. By contrast  $(AuAg)_{267}$  displays 187 free electrons assuming the cluster is neutral. Because this particle is almost spherical, the electronic structure of the metal core is understood by the simplified jellium model. Projected local density of states of the  $(AuAg)_{267}$  cluster models do not display an energy gap of 187 electrons. The electronic structure does not have any primary mechanism to stabilize the atomic structure of  $(AuAg)_{267}$  due to the lack of measurable HOMO–LUMO energy gap. Therefore, the stability must derive from the special geometric arrangement of the metal atoms which lead to the magic Mackay/anti-Mackay icosahedral shells and the protective ligand shell structure, as discussed above. The lack of a certain HOMO–LUMO gap was also evidenced from differential pulse voltammetry (DPV). DPV of a solution of cocrystals exhibited 14 peaks which were evenly spaced, and no detectable HOMO–LUMO gap was seen from the reduction and oxidation peaks (Figure 6B(b)).

UV–vis optical absorption spectra of a mixture of  $(AuAg)_{267}$  and  $(AuAg)_{45}$ , as well as the two separate entities is shown in Figure 6B. Solutions of cocrystals showed a plasmon band at 460 nm, while  $(AuAg)_{45}$  displayed molecule-like features. The contribution of larger nanoparticle is high in the optical spectrum due to its large extinction coefficient.

## 5. Cocrystals Consisted of +ve and –ve Clusters Making a Double Nuclear Ionic Compound

Nanoclusters can bear positive or negative charges; therefore, an obvious question is whether the charged nanoclusters can pack together in crystals by electrostatic forces.<sup>[7,88]</sup> The first attempt was made to answer this question by mixing anionic and cationic  $Au_{25}$  nanoclusters, which had not been successful till now.<sup>[55]</sup> This is likely due to the instability of the positively charged  $Au_{25}$ .<sup>[89]</sup>

He et al., reported the synchronous synthesis of cationic and anionic nanoclusters and the in situ formation of the expected compound via a one-pot reaction.<sup>[55]</sup> Initially, poly-disperse particles were synthesized by reducing a complex of silver and ligands, then they were size focused in presence of gold precursor and excess phosphines. The supernatant solution was subjected to the diffusion of hexane to produce black crystals. SCXRD data suggested that the as-obtained product may be written as  $[Ag_{26}Au(2-EBT)_{18}(PPh_3)_6]^+ [Ag_{24}Au(2-EBT)_{18}]^-$ , a double nanocluster ionic compound (DNIC). Such a material is very interesting as it can be regarded as an ionic compound; however, it is different from normal ionic compounds as both the oppositely charged species are nanoclusters.<sup>[90]</sup> It is important to note that such a type of compound has not been

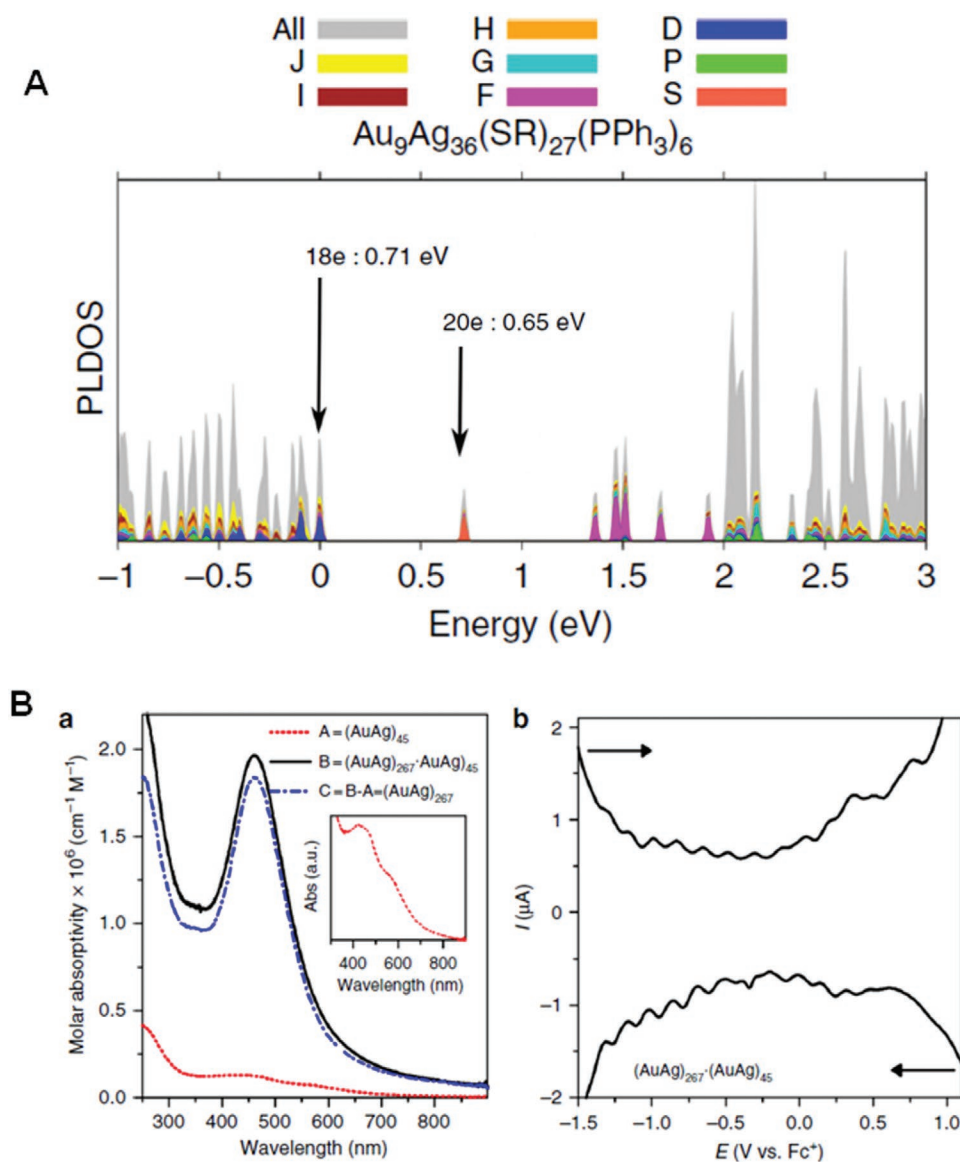


**Figure 6.** A) Predicted electronic structures of  $(\text{AuAg})_{267}$  and  $(\text{AuAg})_{45}$ . The molecules were optimized by density functional theory using coordinates of crystal structure. Energy of the highest occupied molecular orbital (HOMO) was kept at zero. Detectable energy gaps near the HOMO are shown. B,a) Optical absorption spectra of co-crystals and isolated  $(\text{AuAg})_{45}$  in dichloromethane. b) Differential pulse voltammetry of a solution obtained from cocrystals. Reproduced with permission.<sup>[53]</sup> Copyright 2018, Springer Nature.

observed before in a noble metal nanocluster system. Both the clusters,  $\text{Ag}_{26}\text{Au}$  and  $\text{Ag}_{24}\text{Au}$ , do not assemble in an as ion-pair mode but in a layer-by-layer fashion (Figure 7A). Each layer consists of  $\text{Ag}_{26}\text{Au}$  or  $\text{Ag}_{24}\text{Au}$  nanoclusters with a honeycomb-like structure, along the (001) plane (Figure 7B).

Multilayer stacking structure of the cocrystal,  $\text{Ag}_{50}\text{Au}_2$  nanoclusters revealed that besides electrostatic interactions, both the components,  $\text{Ag}_{26}\text{Au}$  and  $\text{Ag}_{24}\text{Au}$  nanoclusters are held together via different supramolecular interactions. These include  $\text{C}-\text{H} \cdots \pi$ , T-shaped  $\pi \cdots \pi$ , and  $\text{H} \cdots \text{H}$  interactions, with distances of 2.8–3.2, 4.8–5.8, and 2.3–2.8 Å, respectively.  $\text{Ag}_{24}\text{Au}(\text{SR})_{18}$  was crystallized separately and the arrangement of the atoms in the single-component nanocluster compound  $[\text{PPh}_4]^+[\text{Ag}_{24}\text{Au}(\text{SR})_{18}]^-$  is similar to that in the cocrystal of

$\text{Ag}_{24}\text{Au}$  of  $\text{Ag}_{50}\text{Au}_2$ , although the supramolecular interactions and packing of  $\text{Ag}_{24}\text{Au}(\text{SR})_{18}$  in the crystals are not the same from the packing of  $\text{Ag}_{24}\text{Au}$  in the crystals. The four benzene rings of each  $\text{PPh}_4$  are bonded with four  $[\text{Ag}_{24}\text{Au}(\text{SR})_{18}]^-$  from the top, and bottom layers by  $\text{C}-\text{H} \cdots \pi$  interactions and the distances are in the range of 2.8–3.1 Å. Thus, it is clear that supramolecular interactions drive the formation of the cocrystal of DNIC, although ionic interactions hold the ion pairs together.

## 6. Conclusions and Perspective

In conclusion, the concept of cocrystallization of structurally similar atomically precise nanoclusters, leading to new solids

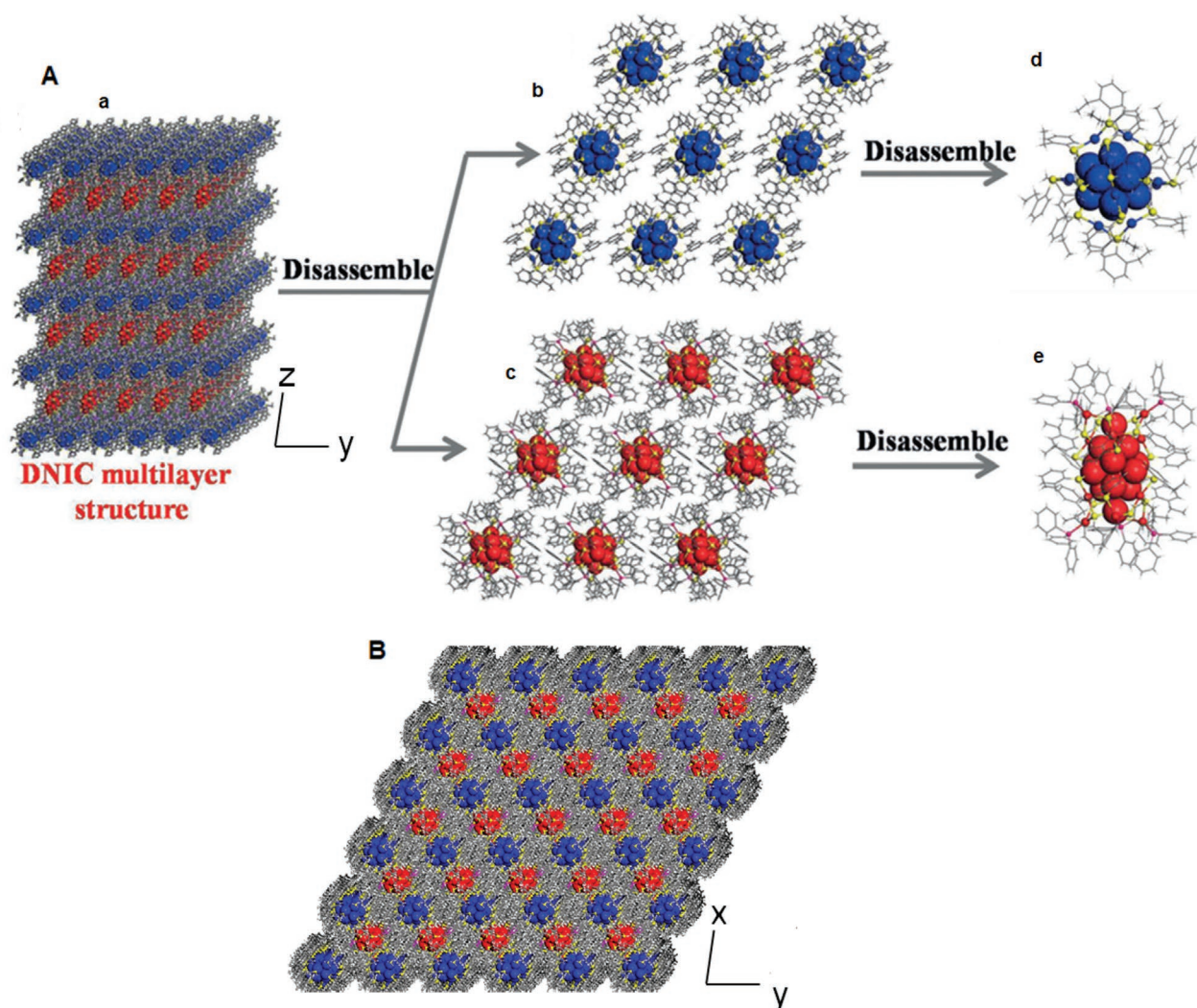


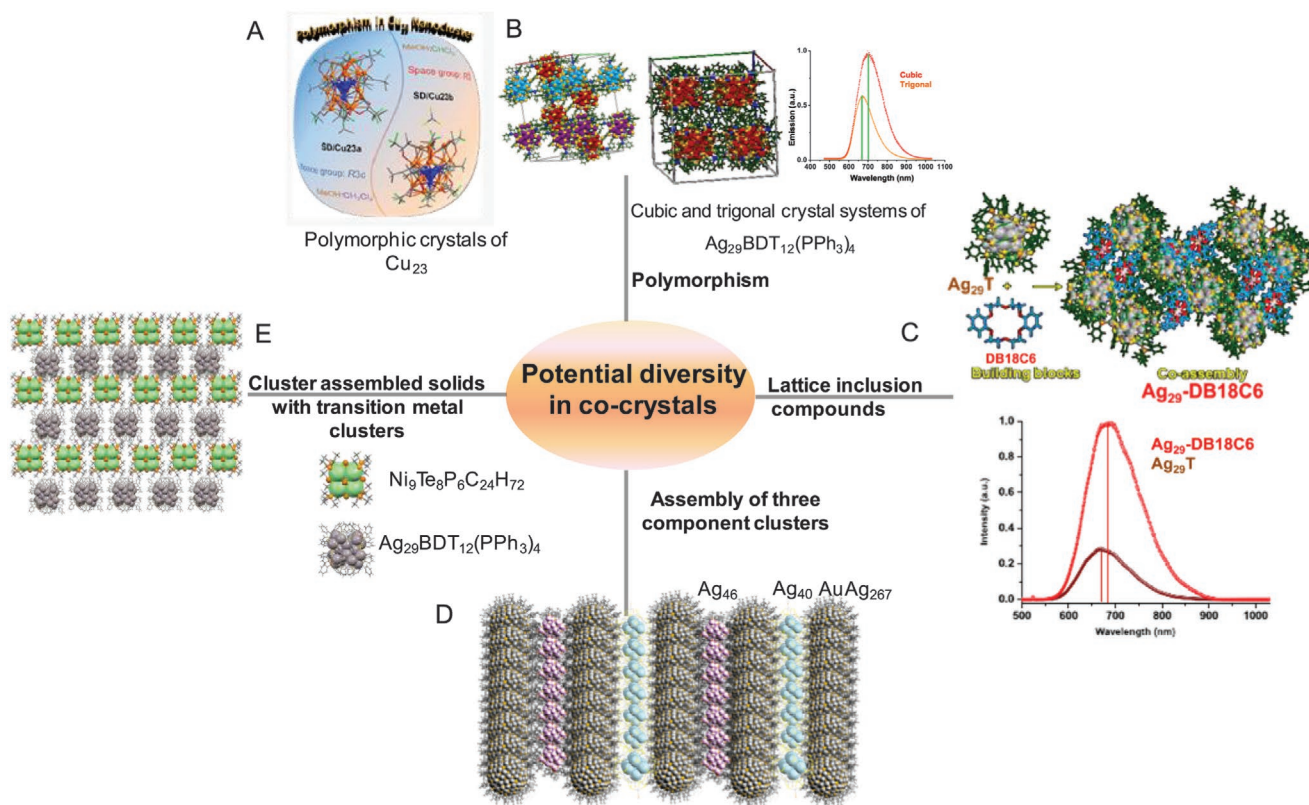
**Figure 7.** A) Demonstration of the coassembly of  $[\text{Ag}_{26}\text{Au}(\text{2-EBT})_{18}(\text{TPP})_6]^+$  and  $[\text{Ag}_{24}\text{Au}(\text{2-EBT})_{18}]^-$ . a) Double ionic cluster ionic compound; Layers of b)  $\text{Ag}_{24}\text{Au}$  and c)  $\text{Au}_{26}\text{Ag}$ ; d) individual  $\text{Ag}_{24}\text{Au}$ , and e)  $\text{Au}_{26}\text{Ag}$  nanoclusters. B) Multilayer stacking structure of the DNIC  $\text{Ag}_{50}\text{Au}_2$  nanoclusters (viewed from Z direction). Color code: blue and red, Ag; yellow, S; magenta, P; gray, C; white, H. Reproduced with permission.<sup>[39]</sup> Copyright 2019, Wiley-VCH.

by different approaches is presented. Five distinct categories of assemblies were presented. 1) Crystals composed of different cores with the same shell. A unique pair of  $\text{Ag}_{40}$  and  $\text{Ag}_{46}$  was cocrystallized with this strategy. 2) Clusters of the same number of metal atoms in the core. An example known is the large metallic shell-like Russian-doll,  $\text{Ag}_{19}@\text{Ag}_{52}@\text{Ag}_{45}@\text{Ag}_{89}$  (in total,  $\text{Ag}_{205}$ ) containing clusters, covered by the same number of thiolates and chloride ligands but different number of silver-phosphine complex units, crystallized together. 3) Another class is an interparticle reaction of two ligand protected atomically precise NCs,  $\text{Ag}_{12}$  and  $\text{Ag}_{18}$  forming products,  $\text{Ag}_{16}$  and  $\text{Ag}_{17}$ , which crystallized together. Detailed analysis revealed that the population of  $\text{Ag}_{16}$  and  $\text{Ag}_{17}$  formed initially in the solution was almost equal, but selective encapsulation happened in the solid state. 4) Coassembly of large and small clusters, example being large  $(\text{AuAg})_{267}$  and tiny  $(\text{AuAg})_{45}$  clusters, assembled into a two-component hierarchical structure. It exemplified a unique particle growth from solution, driven by magic sizes and stable electronically closed-shells. Particularly,  $(\text{AuAg})_{267}$  acquired a magic size close packing, while  $(\text{AuAg})_{45}$  had a 18

electron superatom structure. 5) The idea of a double ionic cluster assembly was introduced by the system,  $[\text{Ag}_{26}\text{Au}(\text{2-EBT})_{18}(\text{PPh}_3)_6]^+ [\text{Ag}_{24}\text{Au}(\text{2-EBT})_{18}]^-$  through an in situ cluster growth approach.

These examples suggest the possibility of the coexistence of diverse clusters and their cocrystallisation in varying ways. Such nanomaterials, like superlattices might be a step forward to understand cluster assembled materials with exciting properties. Interesting cluster solids may be made with combinations of luminescent and nonluminescent clusters, magnetic and nonmagnetic clusters as well as plasmonic and luminescent clusters. Cocrystals of anisotropic and isotropic clusters may also be possible. These new solids may help us understand the synergistic effects of individual clusters.

The diversity of atomically precise clusters is quite large, and it presents potential directions for the future to create new solids. Polymorphic crystals of nanoclusters were introduced by our group.<sup>[63]</sup> It is highly possible to create polymorphism in cocrystals of nanoclusters which may exhibit new electronic properties. So far most of the studies were of binary systems.



**Scheme 4.** A schematic representation of potential diversity in cocrystals of atomically precise clusters. A) Reproduced with permission.<sup>[93]</sup> Copyright 2020, American Chemical Society. B) Reproduced with permission.<sup>[63]</sup> Copyright 2018, The Royal Society of Chemistry. C) Reproduced with permission.<sup>[92]</sup> Copyright 2019, American Chemical Society.

It will be interesting if we can realize multicomponent cluster cocrystals. Recently, three superatom alloy and pure clusters were crystallized together.<sup>[91]</sup> Multicomponent solids may have exciting physicochemical, electrical, and mechanical properties, which will help the growth of this very new field. Our group reported a supramolecular assembly of  $\text{Ag}_{29}$  clusters and crown ether<sup>[92]</sup> which suggests possibilities of cocrystallizing different clusters by suitable supramolecular building blocks. Another exciting possibility is to combine noble metal nanoclusters with clusters of transition metals. Let us take an interesting example of a cocrystal of magnetic  $\text{Ni}_9$  clusters<sup>[50]</sup> with luminescent  $\text{Ag}_{29}$  clusters.<sup>[6]</sup> This kind of materials may give completely new properties and can amplify their existing properties. Several of these possibilities are summarized in **Scheme 4**.

In our opinion, the major challenge to create such solids is to create generalized approaches for diverse building blocks. A critically limiting factor in assembling clusters is the fast interparticle reactivity and diffusion of atoms, which are significant at this length scale.<sup>[20,94]</sup> We believe that different research groups across the world will take initiatives to take this newly growing field to greater heights. The prime motive to create such assemblies will be the potentially interesting properties of such materials, such as a combination of luminescence and magnetism, luminescence and chirality, etc. It is important to recall that molecular clusters, such as  $\text{C}_{60}$  completely new properties, such as superconductivity and magnetism by forming charge-transfer complexes.

The driving force for cocrystallization might be the stability of multicomponent systems. Mechanism of cocrystal

formation is not clear yet. Possibly, it largely depends on the geometric and electronic structures of the component clusters. Detailed mechanism of such cluster growth and their encapsulation in a single crystal would need additional studies. New directions of these materials will also depend on the power of experimental and computational methods that can be developed in the coming years to understand emergent phenomena.

## Acknowledgements

The authors thank the Department of Science and Technology (DST) for supporting the research program. M.B. thanks U.G.C. for his research fellowship. W.A.D. thanks SERB-DST for the award of a National Postdoctoral Fellowship (NPDF).

## Conflict of Interest

The authors declare no conflict of interest.

## Keywords

cluster crystals, cocrystals, crystallization, nanoclusters

Received: July 1, 2020

Revised: August 21, 2020

Published online:

- [1] I. Chakraborty, T. Pradeep, *Chem. Rev.* **2017**, *117*, 8208.
- [2] R. Jin, C. Zeng, M. Zhou, Y. Chen, *Chem. Rev.* **2016**, *116*, 10346.
- [3] P. D. Jadzinsky, G. Calero, C. J. Ackerson, D. A. Bushnell, R. D. Kornberg, *Science* **2007**, *318*, 430.
- [4] M. Zhu, C. M. Aikens, F. J. Hollander, G. C. Schatz, R. Jin, *J. Am. Chem. Soc.* **2008**, *130*, 5883.
- [5] N. Yan, N. Xia, L. Liao, M. Zhu, F. Jin, R. Jin, Z. Wu, *Sci. Adv.* **2018**, *4*, eaat7259.
- [6] L. G. AbdulHalim, M. S. Bootharaju, Q. Tang, S. Del Gobbo, R. G. AbdulHalim, M. Eddaoudi, D.-e. Jiang, O. M. Bakr, *J. Am. Chem. Soc.* **2015**, *137*, 11970.
- [7] A. Desireddy, B. E. Conn, J. Guo, B. Yoon, R. N. Barnett, B. M. Monahan, K. Kirschbaum, W. P. Griffith, R. L. Whetten, U. Landman, T. P. Bigioni, *Nature* **2013**, *501*, 399.
- [8] T.-Q. Yang, B. Peng, B.-Q. Shan, Y.-X. Zong, J.-G. Jiang, P. Wu, K. Zhang, *J. Nanomater.* **2020**, *10*, 261.
- [9] A. Mathew, E. Varghese, S. Choudhury, S. K. Pal, T. Pradeep, *Nanoscale* **2015**, *7*, 14305.
- [10] I. Diez, R. H. A. Ras, *Nanoscale* **2011**, *3*, 1963.
- [11] A. Mathew, T. Pradeep, *Part. Part. Syst. Charact.* **2014**, *31*, 1017.
- [12] M. Brust, J. Fink, D. Bethell, D. J. Schiffrin, C. Kiely, *J. Chem. Soc., Chem. Commun.* **1995**, 1655.
- [13] M. Brust, M. Walker, D. Bethell, D. J. Schiffrin, R. Whyman, *Chem. Soc., Chem. Commun.* **1994**, 0, 801.
- [14] K. R. Krishnadas, D. Ghosh, A. Ghosh, G. Natarajan, T. Pradeep, *J. Phys. Chem. C* **2017**, *121*, 23224.
- [15] Z.-J. Guan, J.-L. Zeng, Z.-A. Nan, X.-K. Wan, Y.-M. Lin, Q.-M. Wang, *Sci. Adv.* **2016**, *2*, e1600323.
- [16] E. Khatun, M. Bodiuzzaman, K. S. Sugi, P. Chakraborty, G. Paramasivam, W. A. Dar, T. Ahuja, S. Antharjanam, T. Pradeep, *ACS Nano* **2019**, *13*, 5753.
- [17] X. Kang, S. Wang, M. Zhu, *Chem. Sci.* **2018**, *9*, 3062.
- [18] E. Khatun, A. Ghosh, P. Chakraborty, P. Singh, M. Bodiuzzaman, P. Ganesan, G. Natarajan, J. Ghosh, S. K. Pal, T. Pradeep, *Nanoscale* **2018**, *10*, 20033.
- [19] A. Ghosh, O. F. Mohammed, O. M. Bakr, *Acc. Chem. Res.* **2018**, *51*, 3094.
- [20] K. R. Krishnadas, A. Baksi, A. Ghosh, G. Natarajan, A. Som, T. Pradeep, *Acc. Chem. Res.* **2017**, *50*, 1988.
- [21] Q. Yao, Y. Feng, V. Fung, Y. Yu, D.-e. Jiang, J. Yang, J. Xie, *Nat. Commun.* **2017**, *8*, 1555.
- [22] Y. Du, H. Sheng, D. Astruc, M. Zhu, *Chem. Rev.* **2020**, *120*, 526.
- [23] S. Zhao, R. Jin, H. Abroshan, C. Zeng, H. Zhang, S. D. House, E. Gottlieb, H. J. Kim, J. C. Yang, R. Jin, *J. Am. Chem. Soc.* **2017**, *139*, 1077.
- [24] L. Zhang, E. Wang, *Nano Today* **2014**, *9*, 132.
- [25] A. Mathew, P. R. Sajanlal, T. Pradeep, *Angew. Chem., Int. Ed.* **2012**, *51*, 9596.
- [26] L.-Y. Chen, C.-W. Wang, Z. Yuan, H.-T. Chang, *Anal. Chem.* **2015**, *87*, 216.
- [27] J. Fang, B. Zhang, Q. Yao, Y. Yang, J. Xie, N. Yan, *Coord. Chem. Rev.* **2016**, *322*, 1.
- [28] M. Schulz-Dobrick, M. Jansen, *Eur. J. Inorg. Chem.* **2006**, *2006*, 4498.
- [29] S. A. Claridge, A. W. Castleman, S. N. Khanna, C. B. Murray, A. Sen, P. S. Weiss, *ACS Nano* **2009**, *3*, 244.
- [30] X. Roy, C.-H. Lee, A. C. Crowther, C. L. Schenck, T. Besara, R. A. Lalancette, T. Siegrist, P. W. Stephens, L. E. Brus, P. Kim, M. L. Steigerwald, C. Nuckolls, *Science* **2013**, *341*, 157.
- [31] E. J. Telford, J. C. Russell, J. R. Swann, B. Fowler, X. Wang, K. Lee, A. Zangiabadi, K. Watanabe, T. Taniguchi, C. Nuckolls, P. Batail, X. Zhu, J. A. Malen, C. R. Dean, *X. Roy, Nano Lett.* **2020**, *20*, 1718.
- [32] A. Nag, P. Chakraborty, G. Paramasivam, M. Bodiuzzaman, G. Natarajan, T. Pradeep, *J. Am. Chem. Soc.* **2018**, *140*, 13590.
- [33] A. Mathew, G. Natarajan, L. Lehtovaara, H. Häkkinen, R. M. Kumar, V. Subramanian, A. Jaleel, T. Pradeep, *ACS Nano* **2014**, *8*, 139.
- [34] J.-R. Wang, Q. Yu, W. Dai, X. Mei, *Chem. Commun.* **2016**, *52*, 3572.
- [35] J. F. Remenar, S. L. Morissette, M. L. Peterson, B. Moulton, J. M. MacPhee, H. R. Guzmán, Ö. Almarsson, *J. Am. Chem. Soc.* **2003**, *125*, 8456.
- [36] C. B. Aakeröy, S. Forbes, J. Desper, *J. Am. Chem. Soc.* **2009**, *131*, 17048.
- [37] R. D. B. Walsh, M. W. Bradner, S. Fleischman, L. A. Morales, B. Moulton, N. Rodríguez-Hornedo, M. J. Zaworotko, *Chem. Commun.* **2003**, 186.
- [38] S. L. Childs, L. J. Chyall, J. T. Dunlap, V. N. Smolenskaya, B. C. Stahly, G. P. Stahly, *J. Am. Chem. Soc.* **2004**, *126*, 13335.
- [39] S. Karki, T. Friščić, L. Fábrián, P. R. Laity, G. M. Day, W. Jones, *Adv. Mater.* **2009**, *21*, 3905.
- [40] S. R. Perumalla, L. Shi, C. C. Sun, *CrystEngComm* **2012**, *14*, 2389.
- [41] M. Morimoto, M. Irie, *J. Am. Chem. Soc.* **2010**, *132*, 14172.
- [42] O. Bolton, A. J. Matzger, *Angew. Chem., Int. Ed.* **2011**, *50*, 8960.
- [43] G. Griffini, L. Brambilla, M. Levi, C. Castiglioni, M. Del Zoppo, S. Turri, *RSC Adv.* **2014**, *4*, 9893.
- [44] R. Kaur, S. S. R. R. Perumal, A. J. Bhattacharyya, S. Yashonath, T. N. Guru Row, *Cryst. Growth Des.* **2014**, *14*, 423.
- [45] J. Zhang, P. Gu, G. Long, R. Ganguly, Y. Li, N. Aratani, H. Yamada, Q. Zhang, *Chem. Sci.* **2016**, *7*, 3851.
- [46] S. Ghosh, C. M. Reddy, *Angew. Chem., Int. Ed.* **2012**, *51*, 10319.
- [47] A. Delori, A. J. Urquhart, I. D. H. Oswald, *CrystEngComm* **2016**, *18*, 5360.
- [48] M. Schulz-Dobrick, M. Jansen, *Inorg. Chem.* **2007**, *46*, 4380.
- [49] L. Wang, T. Wu, X. Bu, X. Zhao, F. Zuo, P. Feng, *Inorg. Chem.* **2013**, *52*, 2259.
- [50] A. Turkiewicz, D. W. Paley, T. Besara, G. Elbaz, A. Pinkard, T. Siegrist, X. Roy, *J. Am. Chem. Soc.* **2014**, *136*, 15873.
- [51] J.-Y. Liu, F. Alkan, Z. Wang, Z.-Y. Zhang, M. Kurmoo, Z. Yan, Q.-Q. Zhao, C. M. Aikens, C.-H. Tung, D. Sun, *Angew. Chem., Int. Ed.* **2019**, *58*, 195.
- [52] M. Bodiuzzaman, A. Ghosh, K. S. Sugi, A. Nag, E. Khatun, B. Varghese, G. Paramasivam, S. Antharjanam, G. Natarajan, T. Pradeep, *Angew. Chem., Int. Ed.* **2019**, *58*, 189.
- [53] J. Yan, S. Malola, C. Hu, J. Peng, B. Dittrich, B. K. Teo, H. Häkkinen, L. Zheng, N. Zheng, *Nat. Commun.* **2018**, *9*, 3357.
- [54] W. A. Dar, M. Bodiuzzaman, D. Ghosh, G. Paramasivam, E. Khatun, K. S. Sugi, T. Pradeep, *ACS Nano* **2019**, *13*, 13365.
- [55] L. He, Z. Gan, N. Xia, L. Liao, Z. Wu, *Angew. Chem., Int. Ed.* **2019**, *58*, 9897.
- [56] C. Zeng, H. Qian, T. Li, G. Li, N. L. Rosi, B. Yoon, R. N. Barnett, R. L. Whetten, U. Landman, R. Jin, *Angew. Chem., Int. Ed.* **2012**, *51*, 13114.
- [57] H. Yang, J. Yan, Y. Wang, H. Su, L. Gell, X. Zhao, C. Xu, B. K. Teo, H. Häkkinen, N. Zheng, *J. Am. Chem. Soc.* **2017**, *139*, 31.
- [58] C. Liu, T. Li, H. Abroshan, Z. Li, C. Zhang, H. J. Kim, G. Li, R. Jin, *Nat. Commun.* **2018**, *9*, 744.
- [59] W. Du, S. Jin, L. Xiong, M. Chen, J. Zhang, X. Zou, Y. Pei, S. Wang, M. Zhu, *J. Am. Chem. Soc.* **2017**, *139*, 1618.
- [60] A. Dass, S. Theivendran, P. R. Nimmala, C. Kumara, V. R. Jupally, A. Fortunelli, L. Sementa, G. Barcaro, X. Zuo, B. C. Noll, *J. Am. Chem. Soc.* **2015**, *137*, 4610.
- [61] J. Chai, S. Yang, Y. Lv, T. Chen, S. Wang, H. Yu, M. Zhu, *J. Am. Chem. Soc.* **2018**, *140*, 15582.
- [62] C. P. Joshi, M. S. Bootharaju, M. J. Alhilaly, O. M. Bakr, *J. Am. Chem. Soc.* **2015**, *137*, 11578.
- [63] A. Nag, P. Chakraborty, M. Bodiuzzaman, T. Ahuja, S. Antharjanam, T. Pradeep, *Nanoscale* **2018**, *10*, 9851.
- [64] Y. Shichibu, Y. Negishi, T. Watanabe, N. K. Chaki, H. Kawaguchi, T. Tsukuda, *J. Phys. Chem. C* **2007**, *111*, 7845.
- [65] H. Häkkinen, M. Walter, H. Grönbeck, *J. Phys. Chem. B* **2006**, *110*, 9927.
- [66] M. J. Alhilaly, M. S. Bootharaju, C. P. Joshi, T. M. Besong, A.-H. Erwas, R. Juarez-Mosqueda, S. Kaappa, S. Malola, K. Adil,

- A. Shkurenko, H. Häkkinen, M. Eddaoudi, O. M. Bakr, *J. Am. Chem. Soc.* **2016**, *138*, 14727.
- [67] E. G. Mednikov, L. F. Dahl, *Small* **2008**, *4*, 534.
- [68] R. Jin, Y. Zhu, H. Qian, *Chem. – Eur. J.* **2011**, *17*, 6584.
- [69] C. Liu, T. Li, G. Li, K. Nobusada, C. Zeng, G. Pang, N. L. Rosi, R. Jin, *Angew. Chem., Int. Ed.* **2015**, *54*, 9826.
- [70] M. Walter, J. Akola, O. Lopez-Acevedo, P. D. Jadzinsky, G. Calero, C. J. Ackerson, R. L. Whetten, H. Grönbeck, H. Häkkinen, *Proc. Natl. Acad. Sci. USA* **2008**, *105*, 9157.
- [71] X. Kang, F. Xu, X. Wei, S. Wang, M. Zhu, *Sci. Adv.* **2019**, *5*, eaax7863.
- [72] K. R. Krishnadas, A. Ghosh, A. Baksi, I. Chakraborty, G. Natarajan, T. Pradeep, *J. Am. Chem. Soc.* **2016**, *138*, 140.
- [73] Z. Gan, N. Xia, Z. Wu, *Acc. Chem. Res.* **2018**, *51*, 2774.
- [74] K. R. Krishnadas, A. Baksi, A. Ghosh, G. Natarajan, T. Pradeep, *Nat. Commun.* **2016**, *7*, 13447.
- [75] K. R. Krishnadas, A. Baksi, A. Ghosh, G. Natarajan, T. Pradeep, *ACS Nano* **2017**, *11*, 6015.
- [76] A. Ghosh, D. Ghosh, E. Khatun, P. Chakraborty, T. Pradeep, *Nanoscale* **2017**, *9*, 1068.
- [77] B. Zhang, O. V. Safonova, S. Pollitt, G. Salassa, A. Sels, R. Kazan, Y. Wang, G. Rupprechter, N. Barrabés, T. Bürgi, *Phys. Chem. Chem. Phys.* **2018**, *20*, 5312.
- [78] M. Suyama, S. Takano, T. Nakamura, T. Tsukuda, *J. Am. Chem. Soc.* **2019**, *141*, 14048.
- [79] B. Zhang, G. Salassa, T. Bürgi, *Chem. Commun.* **2016**, *52*, 9205.
- [80] *Protected Metal Clusters: From Fundamentals to Applications*, (Eds: T. Tsukuda, H. Hakkinen) Elsevier Ltd., Oxford **2015**, *9*, 357.
- [81] A. L. Mackay, *Acta Crystallogr.* **1962**, *15*, 916.
- [82] N. T. Tran, D. R. Powell, L. F. Dahl, *Angew. Chem., Int. Ed.* **2000**, *39*, 4121.
- [83] E. G. Mednikov, M. C. Jewell, L. F. Dahl, *J. Am. Chem. Soc.* **2007**, *129*, 11619.
- [84] C. Zeng, Y. Chen, K. Kirschbaum, K. Appavoo, M. Y. Sfeir, R. Jin, *Sci. Adv.* **2015**, *1*, e1500045.
- [85] J. D. Erickson, E. G. Mednikov, S. A. Ivanov, L. F. Dahl, *J. Am. Chem. Soc.* **2016**, *138*, 1502.
- [86] K. H. Kuo, *J. Struct. Chem.* **2002**, *13*, 221.
- [87] L. Liao, S. Zhuang, P. Wang, Y. Xu, N. Yan, H. Dong, C. Wang, Y. Zhao, N. Xia, J. Li, H. Deng, Y. Pei, S.-K. Tian, Z. Wu, *Angew. Chem., Int. Ed.* **2017**, *56*, 12644.
- [88] C. M. Aikens, *J. Phys. Chem. C* **2008**, *112*, 19797.
- [89] Z. Wu, R. Jin, *Nano Lett.* **2010**, *10*, 2568.
- [90] Z. Wu, R. Jin, *Chem. – Eur. J.* **2011**, *17*, 13966.
- [91] J.-H. Liao, S. Kahlal, Y.-C. Liu, M.-H. Chiang, J.-Y. Saillard, C. W. Liu, *J. Cluster Sci.* **2018**, *29*, 827.
- [92] P. Chakraborty, A. Nag, K. S. Sugi, T. Ahuja, B. Varghese, T. Pradeep, *ACS Mater. Lett.* **2019**, *1*, 534.
- [93] B.-L. Han, Z. Liu, L. Feng, Z. Wang, R. K. Gupta, C. M. Aikens, C.-H. Tung, D. Sun, *J. Am. Chem. Soc.* **2020**, *142*, 5834.
- [94] K. R. Krishnadas, G. Natarajan, A. Baksi, A. Ghosh, E. Khatun, T. Pradeep, *Langmuir* **2019**, *35*, 11243.